The fate of carbon dioxide in water-rich fluids at extreme conditions

Ding Pan^{1*}, Giulia Galli^{1,2}

¹The Institute for Molecular Engineering, the University of Chicago, Chicago, IL 60637, USA

²Argonne National Laboratory, Argonne, IL 60439, USA

* dingpan@uchicago.edu

Investigating the fate of dissolved carbon dioxide under extreme conditions is critical to understanding the deep carbon cycle in the Earth, a process that ultimately influences global climate change. We used first-principles molecular dynamics simulations to study carbonates and carbon dioxide dissolved in water at pressures (P) and temperatures (T) approximating the conditions of the Earth's upper mantle. Contrary to popular geochemical models assuming that molecular $CO_2(aq)$ is the major carbon species present in water under deep earth conditions, we found that at 11 GPa and 1000 K carbon exists almost entirely in the forms of solvated carbonate (CO_3^{2-}) and bicarbonate (HCO_3^{-}) ions, and that even carbonic acid $(H_2CO_3(aq))$ is more abundant than $CO_2(aq)$. Furthermore, our simulations revealed that ion pairing between Na⁺ and CO_3^{2-}/HCO_3^{-} is greatly affected by P-T conditions, decreasing with increasing pressure at $800\sim1000$ K. Our results suggest that in the Earth's upper mantle, water-rich geo-fluids transport a majority of carbon in the form of rapidly interconverting CO_3^{2-} and HCO_3^{-} ions, not solvated

$CO_2(aq)$ molecules.

Introduction

The threat of global warming and climate change makes the understanding of the Earth carbon cycle a critical and pressing task. In the Earth's lithosphere, sedimentary carbonates are considered as the largest carbon hosts [1], with carbon transport between the Earth's surface and interior [2] occurring continuously over millions to billions years [3]. For example, carbon belonging to organic matter and carbonate minerals may go deep into the Earth's mantle within subduction zones, and it may be brought back to the Earth's surface by volcanism through CO₂ degassing [4]. The deep carbon cycle substantially influences the carbon budget near the Earth's surface, which in turn impacts our energy consumption and global climate change [4]. However, whether carbon accumulates in our planet's interior is still the subject of debate, and the chemical reactions leading to the predominant species of carbon in the deep Earth are not yet well understood; hence, the means by which carbon transport occurs within the Earth has not yet been established [2].

Carbon may be transported by crustal and mantle fluids in subduction zones [5], where water is a major transport medium [6]. However the forms of dissolved carbon in water under the deep Earth conditions are poorly known. In the Earth's upper mantle, the pressure (P) may reach ~ 13 GPa and the temperature (T) ~ 1700 K [7]. Experimentally it is challenging to reproduce those conditions and study aqueous solutions of CO_2 and carbonates in the laboratory, because water becomes highly corrosive [8, 9] and it is difficult to obtain clear vibrational spectroscopic signals, which are commonly used to characterize aqueous solutions at ambient conditions. In addition, the interpretation of existing Raman spectra measured at high P-T is controversial, as it is yet unclear how to relate the solute concentration to the observed signals in supercritical conditions [10, 11]. Experimental data have been obtained *either* at high P (HP) or at high T (HT), but it has not yet been possible to reach *both* HP *and* HT, as shown in Fig. 1. Therefore our understanding of the chemistry of aqueous carbon is limited to P-T conditions

of shallow mantle environments [12]. Due to the lack of experimental data, traditional geochemical models were based on several assumptions, one of which is that $CO_2(aq)$ is the major dissolved carbon species in supercritical water under oxidizing conditions(e.g., [13, 14, 15] and references therein).

In this article, by conducting extensive first-principles molecular dynamics (MD) simulations, we studied Na₂CO₃ and CO₂ aqueous solutions at 11 GPa and 1000 K, i.e. at pressures similar to those at the bottom of the Earth's upper mantle. We note that ab initio simulations, which do not require any experimental input, have been shown to be powerful tools to study chemical reactions under extreme conditions [16]. However they are computationally demanding and cannot yet be used to carry out a detailed study of the whole P-T range in the Earth mantle. The present study focuses instead on general properties of dissolved carbon in water under extreme conditions that could not been addressed before by simple models which do not take into account explicitly the molecular nature of water and the way it dissociates under pressure. Contrary to the assumption that CO₂(aq) is the major carbon species under oxidizing conditions, we found that most of the dissolved carbon is in the form of CO_3^{2-} and HCO_3^- , with continuous transformation of the two species into each other on the scale of picoseconds. Surprisingly, even H₂CO₃(aq) is more abundant than CO₂(aq) when CO₂ is directly dissolved into water at 11 GPa and 1000 K. We also found that ion pairing occurs between Na^+ and CO_3^{2-} or HCO₃⁻. Our study confirms that the molecular structure of supercritical water is markedly different from that of the liquid at ambient conditions, and shows that the fast chemical dynamics in aqueous solutions at extreme conditions is key to understanding dissolved carbon in deep geofluids. Our findings suggest that at the bottom of the upper mantle, solvated CO₂(aq) is hardly present in water, with most of the species being carbonate and bicarbonate ions. We expect these highly active ionic species to be involved in the carbon recycle process in subduction zones in the deep Earth, and to play an important role in the transport of carbon.

Results and discussion

Validation of computational strategy—Before carrying out simulations at the Earth's mantle conditions, we validated our computational strategy, in particular we tested the accuracy of exchange-correlation (xc) functionals used in density functional theory (DFT), by simulating a carbonate solution at 0.2 GPa and 823 K, for which experimental spectroscopic studies and geochemical models are available [17]. We considered one Na₂CO₃ molecule and 62 water molecules (molality: 0.9 m) in a cubic simulation box with side length of 14.42 Å. According to Duan et al.'s equations of state [18, 14] which are fitted to experimental data, the density of water in these conditions corresponds to a pressure of \sim 0.2 GPa. We chose sodium as a representative cation since Na₂CO₃ has a large solubility in supercritical water [19, 11, 20]; Na is the seventh most abundant element in the Earth's mantle [21].

Fig. 2(A) shows the mole percents of $CO_2(aq)$, CO_3^{2-} , HCO_3^- and $H_2CO_3(aq)$ species as functions of simulation time in first-principles MD simulations carried out with semilocal (PBE [22]) and hybrid (PBE0 [23]) functionals. The overall mole percents in our extensive MD simulations are summarized in Table. 1. Using PBE, we found that bicarbonate is the dominating carbon species in the solution, with \sim 82 % (mole percent of total dissolved carbon, see also methods) bicarbonate ions and \sim 17% carbonate ions over a \sim 130 ps MD simulation. The amounts of $CO_2(aq)$ and $H_2CO_3(aq)$ were negligible. The lifetime of bicarbonate ions exceeded 10 ps in our simulations while the lifetime of CO_3^{2-} was much shorter.

It is known that generalized gradient approximations (GGA) may not be accurate in the description of solvated doubly charged anions, due to the charge delocalization error [24]. For example, in sulfuric acid aqueous solutions at ambient conditions, Wan et al. found that the concentration of SO_4^{2-} was seriously overestimated when using the PBE functional, while the hybrid functional PBE0, which better describes the charge localization of solvated anions [25], gave results in qualitative agreement with experiments [26, 27, 28]. Hence we compared PBE and PBE0 simulations to extract robust trends from our results. We started a PBE0 simulation from a \sim 40 ps long PBE one. As shown in Fig. 2(A), HCO $_3^-$ ions transformed immediately

into CO_3^{2-} anions. In the subsequent simulation, the total mole percent of HCO_3^- was 27%, indicating that PBE overestimates the concentration of HCO_3^- with respect to PBE0. However, in both PBE and PBE0 simulations we found that few $CO_2(aq)$ or $H_2CO_3(aq)$ molecules were present in the solution at 0.2 GPa and 823 K. Hence the absence of these species in solution was considered to be a robust result of our first-principles MD simulations.

Experimentally, Frantz studied a one-molal K₂CO₃ solution at the same P-T conditions as those considered here, by Raman spectroscopy [10]. The concentration of a given species (C_i) was related to the measured Raman intensity (I_i) by $I_i = \gamma_i C_i$, where γ_i is the Raman scattering cross section. Based on the concentrations calculated by geochemical models, Frantz estimated that the ratio $\frac{\gamma_{carbonate}}{\gamma_{bicarbonate}}$ decreased by ~75% when increasing T from 523 K to 823 K [10]. Recently, after re-examining Frantz's spectroscopic data, Schmidt argued that such ratio should change by less than 10% in that temperature range [11], indicating that the species concentrations obtained by geochemical models in Ref. [10] may be questionable. Our theoretical concentrations are closer to the results obtained by the γ ratio proposed by Schmidt [11] than by Frantz [10]. Using Schmidt's γ ratio and the published Raman spectra [10], we computed the mole percents of oxidized carbon in the solution, and found $68\%~HCO_3^-$ and $32\%~CO_3^{2-}$ (no CO₂(aq) related Raman peaks were reported in Frantz's study). Therefore PBE appears to overestimate the amount of HCO_3^- by $\sim 20\%$ relative to the value obtained from Frantz's spectroscopic data[10] and the γ ratio proposed by Schmidt [11]; however the overestimate is not as serious as, e.g. for sulfuric acid aqueous solutions at ambient conditions [26]. This finding is consistent with our previous investigation of water under pressure, where we found that PBE performs better at extreme than at ambient conditions in terms of equation of state of water, and in predicting static and electronic dielectric constants [20, 29]. On the other hand, our PBE0 simulation yield results much closer to the experimental data. Our validation strategy led us to conclude that the use of the PBE functional is justified at high P and T, where, however, some additional PBE0 simulations were carried out to double check our PBE results.

Absence of $CO_2(aq)$ — The simulations just described led us to question the assumption

of $CO_2(aq)$ being the major carbon species in supercritical aqueous fluids in the deep Earth. We further increased the pressure to ~ 11 GPa and the temperature to 1000 K, i.e. at pressures similar to those at the bottom of the Earth's upper mantle, to investigate whether our conclusions on the absence of $CO_2(aq)$ in water did hold at more extreme conditions. The density of water at this P-T condition is 1.57 g/cm³ [20]. The equation of state of water in this regime has been investigated in our previous study using the PBE functional [20].

Fig. 2(B) shows the mole percentages of dissolved carbon species as functions of simulation time obtained in first-principles MD simulations with the PBE and PBE0 functionals. We found $41\% \text{ CO}_3^{2-}$, $58\% \text{ HCO}_3^{-}$ and $1\% \text{ H}_2\text{CO}_3(\text{aq})$ when using PBE; PBE0 simulations gave $52\% \text{ CO}_3^{2-}$ and $48\% \text{ HCO}_3^{-}$, as shown in Table. 1. Similar to our finding at 0.2 GPa and 823 K, PBE yields a higher concentration of HCO_3^{-} than PBE0, but the results of the two simulations are closer than at lower P and T. Most importantly, less than $1\% \text{ CO}_2(\text{aq})$ was found in both PBE and PBE0 simulations.

Due to the lack of experimental data, many studies at the upper mantle conditions used geochemical models based on extrapolations of available data. Using extrapolated thermodynamic data, Caciagli and Manning considered $CO_2(aq)$ as the dominant dissolved carbon species in calcite aqueous solutions up to 1.6 GPa and 1023 K [30]. Based on geochemical models at lower P and T, Manning et al. inferred that bicarbonate ions would become less favored relative to $CO_2(aq)$ under the mantle conditions [12]. However, Facq et al. performed Raman studies of $CaCO_3$ solutions up to 7 GPa and 673 K, and found that at P > 4 GPa, CO_3^{2-} is the dominant carbon species [31]. Furthermore, based on theoretical models, Facq et al. speculated that at higher temperature $CO_2(aq)$ may become a dominant species, depending on the pressure, though no exact temperature or pressure were reported [31]. In Refs. [30, 31] using solutions at equilibrium with $CaCO_3$ crystals, the concentrations of dissolved carbon are lower than that studied in this work; it is therefore challenging to detect experimentally the amount of $CO_2(aq)$ and definitely rule out the existence of molecular CO_2 . Our first-principles MD simulations clearly showed that up to 11 GPa and 1000 K, few CO_3^{2-} ions are converted to $CO_2(aq)$.

In order to further verify whether $CO_2(aq)$ may be stable in water under extreme conditions, we directly dissolved CO_2 into water at the same P-T condition of the simulation previously described ¹, and found again that only few percent of $CO_2(aq)$ remained after the solution was equilibrated; bicarbonate ions accounted for approximately 80% of dissolved carbon; this result was obtained using both xc functionals as shown in Fig. 2(C).

Interestingly, we also found that $H_2CO_3(aq)$ was present in the solution with a mole percent between 11% and 23%, depending on the functionals; note that this concentration is about 20 times larger than that of of $CO_2(aq)$ as shown in Table. 1. The formation of $H_2CO_3(aq)$ via $CO_2(aq)$ hydration may follow two pathways [32]: 1) $CO_2(aq)$ directly reacts with a water molecule to generate H_2CO_3 (aq); 2) an intermediate HCO_3^- is formed prior to $H_2CO_3(aq)$. At 11 GPa and 1000 K, in both PBE and PBE0 simulations, we found that $H_2CO_3(aq)$ forms after HCO_3^- is formed; however frequent proton hopping events were detected between $H_2CO_3(aq)$ and water. The lifetime of $H_2CO_3(aq)$ is on the subpicosecond scale. The existence of H_2CO_3 was also found in a 55.5 m CO_2 water solution at \sim 32 GPa and 2000 K using first-principles MD with the GGA functional, but no concentration was given due to only a 10 ps simulation at the P-T condition [33].

In aqueous solutions at ambient conditions, $H_2CO_3(aq)$ exists only in a very low concentration and rapidly reverts to $CO_2(aq)$ and water [12]:

$$H_2CO_3(aq) \rightarrow CO_2(aq) + H_2O. \tag{1}$$

Because it is difficult to detect $H_2CO_3(aq)$ at ambient conditions, current geochemical models can not distinguish between $H_2CO_3(aq)$ and $CO_2(aq)$, and $H_2CO_3(aq)$ and $CO_2(aq)$ are modeled as the same species [12]. Our findings, however, point out that this conventional treatment may ignore the important presence of $H_2CO_3(aq)$ as a neutral carbon species in the deep Earth.

 $^{^{1}}$ the carbonate ion was replaced by one CO_{2} molecule and one water molecule in the same simulation box at \sim 11 GPa and 1000 K.

At ambient conditions, the dissociation reaction of $CO_2(aq)$ in pure water:

$$CO_2(aq) + 2H_2O \rightarrow HCO_3^- + H_3O^+$$
 (2)

is rather slow, with an activation free energy of 21.7 kcal/mol (0.94 eV)[34, 32]; more than 99% of CO_2 molecules remain intact when the concentration of CO_2 (aq) is above 0.1 m. However, when the hydroxide ion (OH⁻) is present, the activation free energy of the dissociation of CO_2 (aq) is reduced to 12.0 kcal/mol (0.52 eV). As a result, the dissociation reaction is accelerated dramatically; it is about 10^7 faster than that in pure water [34]. At HP-HT conditions, water molecules are more easily dissociated, producing hydroxide ions, which then react with hydrated CO_2 (aq) thus enhancing its dissociation. The enhanced bending motion of C-O bonds at high P-T also facilitates the change of carbon hybridization from sp to sp^2 . In our simulations, the exact concentrations of charged ions depends on the xc functionals used, but both the GGA and hybrid functionals give the same result on CO_2 (aq) concentration: the latter is negligible in aqueous solutions at 11 GPa and 1000 K. Hence we conclude that our calculations provide strong and robust evidence of the absence of CO_2 (aq) in water at this P-T condition.

Ion pairing— Another important question on the aqueous solutions studied here concerns the interactions between (bi)carbonate ions and metal ions. In Fig. 3, we plotted the radial distribution functions (RDF) and distributions of the C-Na distances obtained from our MD trajectories using the PBE and PBE0 functionals. We first discuss the results given by the two functionals, and we then extract robust features of both simulations.

We examined the solution structures of (bi)carbonate ions in the solutions. In Fig. 3(A), the C-Ow (where Ow denotes an O belonging to water molecules) RDFs obtained by PBE and PBE0 are very similar at 0.2 GPa, 823 K or 11 GPa, 1000 K. At 11 GPa and 1000 K, the first local minimum of the C-Ow RDFs is at ~4.54 Å, corresponding to the separation of the first and second solvation shells of (bi)carbonate ions. Although such a minimum is not easy to define at 0.2 GPa and 823 K, since the first peak of the C-Ow RDFs also appears to vanish at ~4.54 Å, we used the same radial cutoff of 4.54 Å for the first solvation shells of (bi)carbonate ions at two P-T conditions, in order to have a consistent comparison.

The ion pairing strength in an aqueous solution greatly depends on the static dielectric constant of water, ε_0 : the electrostatic interaction between ions in water is $\frac{q_1q_1}{\varepsilon_0r^2}$, where q_1 and q_2 are the electrical charges of the ions, and r is the distance between them. We note that PBE appears to overestimate ε_0 at ambient conditions, while PBE0 yields a result in better agreement with experiment [35]; hence at the PBE level of theory, the overestimate of electrostatic screening leads to a weaker ion pairing, as shown by lower PBE peaks at ~ 3.2 Å in Fig. 3(B). The interesting thing is that under upper mantle pressure conditions, the discrepancy between ε_0 evaluated within PBE and the experimental value is rather small [20], and we expect PBE to yield more realistic ion associations at those conditions than at ambient conditions.

At 0.2 GPa and 823 K, both functionals show marked peaks in the distribution of the C-Na distance at \sim 3.2 Å, indicating strong ion pairing between Na⁺ and CO₃²⁻ or HCO₃⁻. The first peak of the C-Ow RDF is at \sim 3.5 Å, so the Na⁺-CO₃²⁻/HCO₃⁻ pairs tend to reside inside the first solvation shell of (bi)carbonate ions. With increasing P and T to 11 GPa and 1000 K respectively, the main peak of the distribution function of the C-Na distance decreases in intensity, indicating that ion pairing becomes weaker in denser water.

Table 2 shows the mole percents of the ion pairs in the first solvation shells of (bi)carbonate ions. As shown in Table 1 and 2, we found that more than 99% of the CO_3^{2-} anions were accompanied by one or two Na⁺ cations in their first solvation shells at 0.2 GPa and 823 K, while at 11 GPa and 1000 K, less than 63% of the CO_3^{2-} ions had counterions in the first solvation shells. This may be attributed to the change of ε_0 : our previous study showed that with increasing pressure, ε_0 increases along an isotherm [20], and thus the dielectric screening is enhanced, and the electrostatic attraction between Na⁺ and CO_3^{2-} or HCO_3^{-} is weakened. The large dielectric screening also enhances the autoionization of water, producing a higher concentration of OH_1^{-} ions, whose presence accelerates the dissociation of CO_2 .

The pairing of carbonate ions with alkali cations at 0.2 GPa and 823 K was also reported in a one-molal K₂CO₃ solution by using geochemical models [10], but no spectroscopic evidence was available because of the detection limit [10]. Recently, Schmidt reported the Raman spectra,

which were interpreted as showing Na^+ - CO_3^{2-} pairing, for a 1.6 m Na_2CO_3 solution interfaced with quartz at T above 673 K. In the $CaCO_3$ -water-NaCl solutions, Facq et al. interpreted the measured Raman data by assuming the existence of the $NaHCO_3^{\circ}$ complex [36]. In our study, despite the different ion pairing strengths given by the two functionals, we found that ion pairing between Na^+ and CO_3^{2-} or HCO_3^- indeed occurs at 0.2 GPa and 823 K, with its strength decreasing at 11 GPa and 1000 K.

Kinetics of reactions involving CO_3^{2-} and HCO_3^{-} —Bicarbonate and carbonate ions are the major species in the solutions studied here, with frequent proton transfer over ps time scales. Their chemical balance in the Na₂CO₃ solution is:

$$CO_3^{2-} + H_2O \rightleftharpoons HCO_3^- + OH^-. \tag{3}$$

The kinetics of the reaction is key to understanding the chemistry of oxidized carbon in supercritical water.

Fig. 4 shows the distribution of protons hopping between a carbonate ion and its nearest water molecule in the Na₂CO₃ solution at 11 GPa and 1000 K. From Fig. 4, we calculated the effective free energy barrier of proton transfer to the right in the reaction (3) as $\Delta F = -k_B T \ln \frac{P_b}{P_r}$, where P_b and P_r are the probabilities of being on the top of the barrier and in the reactant state, respectively, and k_B is the Boltzmann constant. At the PBE0 level of theory, the free energy barrier is estimated to be 4.6 kcal/mol (0.20 eV), while at the PBE level, it decreases to \sim 2.8 kcal/mol (0.12 eV). According to the Arrhenius equation, the rate constant is Ae^{-E_a/k_BT} , where E_a is the activation energy. If we assume PBE and PBE0 yield a similar prefactor A, and approximate the activation energy by the free energy barrier, the rate constant of the forward reaction (3) using PBE is about three times as large as that found using PBE0. Such a difference may be explained by the difference in O-H bond strengths obtained using the two functionals. We computed the vibrational density of states of the solution at 11 GPa and 1000 K in Fig. S1, and found that the stretching frequency of O-H bonds given by PBE is about 150 cm⁻¹ lower than that obtained with PBE0. As a result, at the PBE level of theory the O-H bond is weaker

and easier to break than at the PBE0 level, and the proton transfer rate is enhanced ².

At T = 1000 K, the thermal energy k_BT is 2.0 kcal/mol (0.086 eV), comparable to the free energy barriers given by PBE and PBE0. Because of the low free energy barrier and enhanced thermal effects, both functionals yield a rate constant of the forward reaction (3) about six orders of magnitude faster than that at ambient conditions ³, indicating highly active ionic interactions in our solutions at 11 GPa and 1000 K.

It is worth noting that Fig. 4 shows only part of the reaction (3); the proton transfer is not only limited to the distance between a carbonate ion and a neighboring water molecule, but it may involve multiple water molecules connected by a hydrogen bond (HB) wire, via a Grotthuss mechanism [39, 40]. In our solutions, protons move back and forth along HB wires over short time scales (<0.1 ps), leading to short-lived (bi)carbonate ions. However, if the thermal fluctuation breaks HB wires, protons can not hop back and then bicarbonate ions persist for few picoseconds. The forming and breaking of the HB wires are critical to the lifetime of carbon species in the calculations reported here.

In Raman experiments, the symmetric stretching mode of C-O/C-OH at $\sim 1000~\rm cm^{-1}$ is used to detect carbonate or bicarbonate ions. The vibrational period of this mode is 33 fs. For the carbon species, whose lifetime is comparable to 33 fs or even shorter, the Raman peaks are broadened considerably, and may be difficult to identify experimentally.

In our MD simulations the forces acting on nuclei were computed quantum mechanically, but protons were still treated as classical particles. If quantum nuclear effects are taken into account, we expect the proton transfer rate to be enhanced, though at such high temperatures quantum effects may not be as important as at ambient conditions [41].

²It has been reported that at ambient conditions the vibrational frequencies of the OH stretching mode are also underestimated using PBE compared with experimental data, whereas PBE0 yields results much closer to experiment [37]. The underestimate decreases with increasing temperature [37]. Those findings suggest that it is necessary to use hybrid functionals to get accurate reaction rates in aqueous solutions, especially at ambient conditions. At extreme conditions, the error of PBE becomes smaller, which is again consistent with the results of our previous studies [20, 29].

 $^{^{3}}$ The rate constant of the forward reaction (3) is 3.06×10^{5} s⁻¹ in sea water at ambient conditions [38].

Using both PBE and PBE0 functionals, van der Waals interactions are described inaccurately; however, in our study we focused on the breaking and forming of covalent bonds and the lack of dispersion forces is not expected to affect our main conclusions. In addition we note that results for the equilibrium volume and dielectric constant of ice obtained with PBE and van der Waals functionals agree much better at high pressure (e.g. for ice VIII) than at low pressure (e.g. for ice Ih and Ic) [43], indicating that the lack of dispersion forces may affect results for water and ice more at ambient conditions than under pressure.

Widely used geochemical models based on the Born function, e.g., the Helgeson–Kirkham–Flowers (HKF) model as implemented in the SUPCRT92 [17], consider water as a continuum medium with no molecular structure taken into account, when calculating thermodynamic properties of electrolytes [44]. In our study we found that the microscopic properties of water at the molecular scale, e.g., proton transfer mechanisms, play a substantial role in the chemical reactions of oxidized carbon, particularly at the high P-T conditions studied here.

Conclusion

In conclusion, we carried out first-principles molecular dynamics simulations to investigate dissolved carbonate and CO_2 in water at high pressure and high temperature, up to the conditions of the Earth's upper mantle. Contrary to popular geochemical models assuming that $CO_2(aq)$ is the major carbon species present in water, we found that most of the dissolved carbon at 11 GPa and 1000 K is in the form of solvated CO_3^{2-} and HCO_3^{-} anions. The two anions exchange protons with water on a picosecond time scale. The proton transfer along hydrogen bond wires driven by thermal fluctuations is responsible for the fast dynamics observed in these solutions. Under such extreme conditions, even $H_2CO_3(aq)$ is more abundant than $CO_2(aq)$, a dramatic difference with respect to ambient conditions. While it is well known that the autoionization of water is greatly enhanced at extreme conditions, e.g., at the P-T conditions of the Earth's mantle, and that the pH of neutral water may be well below 7[6], it has been long unclear how the notable changes of water properties under pressure affect the solvation of oxidized carbon. we

showed, using atomistic ab initio simulations, that the coordination number of carbon changes in water at the Earth's upper mantle conditions. We also found that ion pairing between Na⁺ and CO_3^{2-} or HCO_3^{-} is greatly affected by P-T conditions, decreasing with pressure at 800 \sim 1000 K. Our results suggest that at extreme conditions water transports carbon mostly through highly active ions, not CO_2 (aq) molecules.

The results reported here give important insights into deep carbon science. Our calculations predicted that the carbon dissolved in water-rich geofluids is in ionic forms in the bottom of the Earth's upper mantle, indicating that CO₂ degassing may mostly occur close to the Earth's surface.

Methods

First-principles molecular dynamics (MD) simulations were performed in the Born-Oppenheimer approximation using the Qbox code (http://qboxcode.org/) [45]. Two exchange-correlation (xc) functionals were used: the semilocal functional PBE and the hybrid functional PBE0. In order to improve the efficiency of our calculations using PBE0, the recursive subspace bisection method was used with a threshold of 0.02 [46, 47]. The Brillouin zone of the supercell was sampled with the Γ point only. We used norm-conserving pseudopotentials [48, 49]⁴ with a kinetic cutoff of 85 Ry, which was increased to 220 Ry for pressure calculations. The MD time step was 0.24 fs. Deuterium was used instead of hydrogen, so as to use a larger time step for computational convenience. Note that the density given in the main text was computed for light water. The temperature was maintained constant by the Bussi-Donadio-Parrinello thermostat ($\tau = 24.2 \text{ fs}$)[50].

To determine whether CO_2 or CO_3^{2-} were present in our simulations, we searched the atomic trajectories generated in our simulations for the three closest O atoms to a given C atom, and ordered these O atoms according to their respective C-O distances. If the C-O distance of the

⁴Pseudopotential Table: http://fpmd.ucdavis.edu/potentials

third closest O atom was larger than that of the second one by more than 0.4 Å, the species was considered as CO_2 , otherwise it was defined as a CO_3^{2-} anion. The C-O bond length in all sets of our MD runs was found to be 1.3 ± 0.2 Å. For H atoms around the carbonate ion, we sought the nearest O atom to each of them, and if such O atom belonged to the carbonate ion, we concluded that a bicarbonate ion, HCO_3^- , was formed. When two H atoms were bonded to CO_3^{2-} simultaneously, the solute then became carbonic acid.

Using the criteria described above, we determined the type of solute molecules present in our MD simulations at each time step. Note that at HP-HT conditions, covalent bonds are frequently broken and reformed; hence in order to establish how the concentration of the solute varied along our MD trajectories, we calculated the mole percents of carbon species as functions of simulation time. The mole percent of the *i*th species at time *t* was obtained as:

$$x_i(t) = \frac{n_i(t)}{N_w} \times 100\%,$$
 (4)

where $n_i(t)$ is the number of the snapshots containing the *i*th species between the time $(t - \tau_w)$ and t, and N_w is the total number of snapshots in such a time interval. Here, τ_w was set to 1 ps.

SUPPLEMENTARY MATERIALS

fig. S1. The vibrational density of states of the 0.9 m Na_2CO_3 solution at \sim 11 GPa and 1000 K.

fig. S2. Probability distributions of positions of protons hopping between CO_3^{2-} and H_2O in the Na_2CO_3 solution at 0.2 GPa and 823 K.

Acknowledgements

We thank F. Giberti and D. Gygi for many useful discussions and D. A. Sverjensky for a critical reading of the manuscript and many discussions. This work was supported by the Alfred P. Sloan Foundation through the Deep Carbon Observatory (DCO) and by DOE-BES grant

No. DE-SC0008938. Part of this work was carried out using the DCO Computer Cluster, and resources of the Argonne Leadership Computing Facility (ALCF), provided by an award of computer time by the Innovative and Novel Computational Impact on Theory and Experiment (INCITE) program. ALCF is a DOE Office of Science User Facility supported under Contract DE-AC02-06CH11357. We also acknowledge the University of Chicago Research Computing Center for support of this work.

Contributions

D.P. and G.G. designed the research. Calculations were performed by D.P. All authors contributed to the analysis and discussion of the data and the writing of the manuscript.

Competing Interests

The authors declare that they have no competing interests.

Data and materials availability

All data needed to evaluate the conclusions in the paper are present in the paper and/or the Supplementary Materials. Additional data related to this paper may be requested from the authors.

References

[1] P. Falkowski, *et al.*, The global carbon cycle: a test of our knowledge of earth as a system, *Science* **290**, 291–296 (2000).

- [2] C. E. Manning, Geochemistry: A piece of the deep carbon puzzle, *Nature Geosci.* **7**, 333–334 (2014).
- [3] D. J. DePaolo, Sustainable carbon emissions: The geologic perspective, *MRS Energy & Sustainability* **2**, E9 (2015).
- [4] R. Dasgupta, M. M. Hirschmann, The deep carbon cycle and melting in earth's interior, *Earth Planet. Sci. Lett.* **298**, 1–13 (2010).
- [5] P. B. Kelemen, C. E. Manning, Reevaluating carbon fluxes in subduction zones, what goes down, mostly comes up, *Proc. Natl. Acad. Sci. USA* **112**, E3997–E4006 (2015).
- [6] A. Liebscher, Aqueous fluids at elevated pressure and temperature, *Geofluids* **10**, 3–19 (2010).
- [7] A. B. Thompson, Water in the earth's upper mantle, *Nature* **358**, 295–302 (1992).
- [8] H. Weingärtner, E. U. Franck, Supercritical water as a solvent, *Angew. Chem. Int. Ed. Engl.* 44, 2672–2692 (2005).
- [9] J.-F. Lin, *et al.*, Melting behavior of H₂O at high pressures and temperatures, *Geophysical research letters* **32**, L11306 (2005).
- [10] J. D. Frantz, Raman spectra of potassium carbonate and bicarbonate aqueous fluids at elevated temperatures and pressures: comparison with theoretical simulations, *Chem. Geol.* 152, 211–225 (1998).
- [11] C. Schmidt, Raman spectroscopic determination of carbon speciation and quartz solubility in H₂O+Na₂CO₃ and H₂O+NaHCO₃ fluids to 600 degC and 1.53 GPa, *Geochim. Cosmochim. Acta* **145**, 281–296 (2014).
- [12] C. E. Manning, E. L. Shock, D. Sverjensky, The chemistry of carbon in aqueous fluids at crustal and upper mantle conditions: experimental and theoretical constraints, *Rev. Mineral Geochem.* **75**, 109–148 (2013).

- [13] Z. Duan, Z. Zhang, Equation of state of the H₂O, CO₂, and H₂O–CO₂ systems up to 10 GPa and 2573.15 K: Molecular dynamics simulations with ab initio potential surface, *Geochim. Cosmochim. Acta* **70**, 2311–2324 (2006).
- [14] C. Zhang, Z. Duan, A model for COH fluid in the earth's mantle, *Geochim. Cosmochim. Acta* **73**, 2089–2102 (2009).
- [15] J.-M. Huizenga, Thermodynamic modelling of C–O–H fluids, *Lithos* **55**, 101–114 (2001).
- [16] F. Gygi, G. Galli, Ab initio simulation in extreme conditions, *Mater. Today* **8**, 26–32 (2005).
- [17] J. W. Johnson, E. H. Oelkers, H. C. Helgeson, SUPCRT92: A software package for calculating the standard molal thermodynamic properties of minerals, gases, aqueous species, and reactions from 1 to 5000 bar and 0 to 1000 degC, *Comput. Geosci.* 18, 899–947 (1992).
- [18] Z. Zhang, Z. Duan, Prediction of the *PVT* properties of water over wide range of temperatures and pressures from molecular dynamics simulation, *Phys. Earth Planet Inter.* **149**, 335–354 (2005).
- [19] I. Martinez, C. Sanchez-Valle, I. Daniel, B. Reynard, High-pressure and high-temperature raman spectroscopy of carbonate ions in aqueous solution, *Chem. Geol.* **207**, 47–58 (2004).
- [20] D. Pan, L. Spanu, B. Harrison, D. A. Sverjensky, G. Galli, Dielectric properties of water under extreme conditions and transport of carbonates in the deep earth, *Proc. Natl. Acad. Sci. USA* 110, 6646–6650 (2013).
- [21] I. Jackson, *The Earth's mantle: composition, structure, and evolution* (Cambridge University Press, 2000).

- [22] J. P. Perdew, K. Burke, M. Ernzerhof, Generalized gradient approximation made simple, *Phys. Rev. Lett.* **77**, 3865 (1996).
- [23] C. Adamo, V. Barone, Toward reliable density functional methods without adjustable parameters: The PBE0 model, *J. Chem. Phys.* **110**, 6158 (1999).
- [24] A. J. Cohen, P. Mori-Sánchez, W. Yang, Insights into current limitations of density functional theory, *Science* **321**, 792–794 (2008).
- [25] A. P. Gaiduk, C. Zhang, F. Gygi, G. Galli, Structural and electronic properties of aqueous nacl solutions from ab initio molecular dynamics simulations with hybrid density functionals, *Chem. Phys. Lett.* **604**, 89–96 (2014).
- [26] Q. Wan, L. Spanu, F. Gygi, G. Galli, Electronic structure of aqueous sulfuric acid from first-principles simulations with hybrid functionals, *J. Phys. Chem. Lett.* **5**, 2562–2567 (2014).
- [27] M. Guidon, F. Schiffmann, J. Hutter, J. Vande Vondele, Ab initio molecular dynamics using hybrid density functionals, *J. Chem. Phys.* **128**, 214104 (2008).
- [28] R. A. DiStasio Jr, B. Santra, Z. Li, X. Wu, R. Car, The individual and collective effects of exact exchange and dispersion interactions on the ab initio structure of liquid water, *J. Chem. Phys.* **141**, 084502 (2014).
- [29] D. Pan, Q. Wan, G. Galli, The refractive index and electronic gap of water and ice increase with increasing pressure, *Nat. Commun.* **5**, 3919 (2014).
- [30] N. C. Caciagli, C. E. Manning, The solubility of calcite in water at 6–16 kbar and 500–800 °C, *Contrib. Mineral. Petrol.* **146**, 275–285 (2003).
- [31] S. Facq, I. Daniel, G. Montagnac, H. Cardon, D. A. Sverjensky, In situ raman study and thermodynamic model of aqueous carbonate speciation in equilibrium with aragonite under subduction zone conditions, *Geochim. Cosmochim. Acta* **132**, 375–390 (2014).

- [32] A. Stirling, I. Pápai, H₂CO₃ forms via HCO₃⁻ in water, *J. Phys. Chem. B* **114**, 16854–16859 (2010).
- [33] J.-B. Maillet, E. Bourasseau, Ab initio simulations of thermodynamic and chemical properties of detonation product mixtures., *J. Chem. Phys.* **131**, 084107 (2009).
- [34] X. Wang, W. Conway, R. Burns, N. McCann, M. Maeder, Comprehensive study of the hydration and dehydration reactions of carbon dioxide in aqueous solution, *J. Phys. Chem.* A 114, 1734–1740 (2009).
- [35] M. Schönherr, B. Slater, J. Hutter, J. VandeVondele, Dielectric properties of water ice, the ice Ih/XI phase transition, and an assessment of density functional theory, *J. Phys. Chem. B* **118**, 590–596 (2014).
- [36] S. Facq, I. Daniel, G. Montagnac, H. Cardon, D. A. Sverjensky, Carbon speciation in saline solutions in equilibrium with aragonite at high pressure, *Chemical Geology* **431**, 44–53 (2016).
- [37] C. Zhang, D. Donadio, F. Gygi, G. Galli, First principles simulations of the infrared spectrum of liquid water using hybrid density functionals, *J. Chem. Theory Comput.* **7**, 1443–1449 (2011).
- [38] K. G. Schulz, U. Riebesell, B. Rost, S. Thoms, R. Zeebe, Determination of the rate constants for the carbon dioxide to bicarbonate inter-conversion in pH-buffered seawater systems, *Marine Chemistry* **100**, 53–65 (2006).
- [39] D. Marx, Proton transfer 200 years after von grotthuss: Insights from ab initio simulations, *ChemPhysChem* **7**, 1848–1870 (2006).
- [40] P. L. Geissler, C. Dellago, D. Chandler, J. Hutter, M. Parrinello, Autoionization in liquid water, *Science* **291**, 2121–2124 (2001).

- [41] M. Ceriotti, J. Cuny, M. Parrinello, D. E. Manolopoulos, Nuclear quantum effects and hydrogen bond fluctuations in water, *Proc. Natl. Acad. Sci. USA* **110**, 15591–15596 (2013).
- [42] B. Santra, et al., Hydrogen bonds and van der waals forces in ice at ambient and high pressures, *Phys. Rev. Lett.* **107**, 185701 (2011).
- [43] E. D. Murray, G. Galli, Dispersion interactions and vibrational effects in ice as a function of pressure: A first principles study, *Phys. Rev. Lett.* **108**, 105502 (2012).
- [44] G. M. Anderson, *Thermodynamics of Natural Systems*, 2nd Edition (Cambridge University Press, New York, 2005).
- [45] F. Gygi, Architecture of qbox: A scalable first-principles molecular dynamics code, *IBM J. Res. Dev.* **52**, 137–144 (2008).
- [46] F. Gygi, Compact representations of kohn-sham invariant subspaces, *Phys. Rev. Lett.* **102**, 166406 (2009).
- [47] F. Gygi, I. Duchemin, Efficient computation of hartree–fock exchange using recursive subspace bisection, *J Chem. Theory Comput.* **9**, 582–587 (2012).
- [48] D. R. Hamann, M. Schlüter, C. Chiang, Norm-conserving pseudopotentials, *Phys. Rev. Lett.* **43**, 1494–1497 (1979).
- [49] D. Vanderbilt, Optimally smooth norm-conserving pseudopotentials, *Phys. Rev. B* **32**, 8412–8415 (1985).
- [50] G. Bussi, D. Donadio, M. Parrinello, Canonical sampling through velocity rescaling, *J. Chem. Phys.* **126**, 014101 (2007).
- [51] F. Datchi, P. Loubeyre, R. LeToullec, Extended and accurate determination of the melting curves of argon, helium, ice (H₂O), and hydrogen (H₂), *Phys. Rev. B* **61**, 6535 (2000).

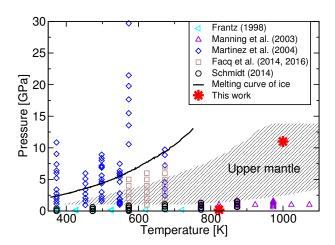


Figure 1: High pressure and high temperature conditions reached in experiments on dissolved carbon in supercritical water, together with the conditions simulated in the present work: Frantz (1998)[10], Manning et al. (2003)[30], Martinez et al. (2004) [19], Facq et al. (2014, 2016) [31, 36], and Schmidt (2014) [11]. The melting curve of ice is from Ref. [51]. The shaded area shows the P-T conditions of the upper mantle [7].

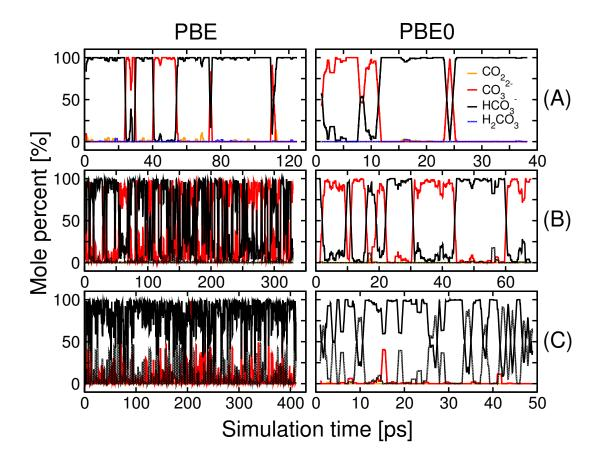


Figure 2: Mole percents of $CO_2(orange)$, $CO_3^{2-}(red)$, $HCO_3^{-}(black)$ and $H_2CO_3(blue)$ as functions of simulation time in first-principles molecular dynamics simulations. (A) 0.9 m (molality) Na_2CO_3 solution at 0.2 GPa and 823 K; (B) 0.9 m Na_2CO_3 solution at 11 GPa and 1000 K; (C) 0.9 m CO_2 solution at 11 GPa and 1000 K. Calculations carried out with two exchange-correlation functionals: PBE [22] and PBE0 [23] are compared.

Table 1: Carbon species in the $0.9 \text{ m Na}_2\text{CO}_3$ and 0.9 m CO_2 solutions in first-principles molecular dynamics simulations. The concentrations are shown as mole percents of the total dissolved carbon. The mole percents of CO_3^{2-} and HCO_3^{-} include those of ion pairs formed by them, respectively. The experimental results (Expt.) are from the Raman data in Ref. [10] (see text).

Solution	P[GPa]	T[K]	Method	Carbon species [%]			
				CO ₂	CO_3^{2-}	HCO_3^-	H ₂ CO ₃
Na ₂ CO ₃	0.2	823	PBE	0.6	16.7	82.4	0.1
			PBE0	0.2	26.8	72.9	0.1
			Expt.	N/A	32	68	N/A
	11	1000	PBE	0.1	40.8	57.9	1.2
			PBE0	0.1	51.8	47.5	0.6
CO ₂	11	1000	PBE	0.6	8.2	79.8	11.4
			PBE0	0.0	1.7	75.0	23.3

Table 2: The ion pairing in the first solvation shells of the carbon species in the 0.9 m Na₂CO₃ solutions. The concentrations are shown as mole percents of the *total* dissolved carbon.

P[GPa]	T[K]	Method	Ion pairing species [%]				
			NaCO ₃	$Na_2CO_3^{\circ}$	NaHCO ₃ °	$Na_2HCO_3^+$	
0.2	823	PBE	3.7	13.0	59.7	7.5	
		PBE0	8.4	18.2	40.8	18.2	
11	1000	PBE	18.1	5.9	28.9	7.5	
		PBE0	22.4	10.0	20.4	12.5	

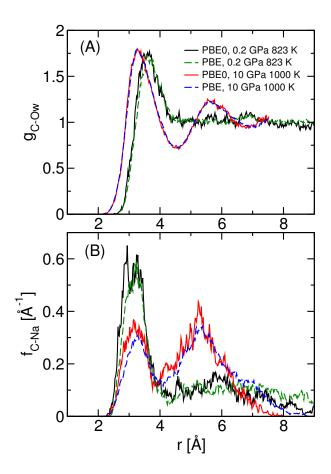


Figure 3: (A) Radial distribution functions (RDF) of carbon atoms (C) vs. oxygen atoms of water (O_w) . (B) Probability distributions of the distances between carbon atoms and sodium ions. The MD simulations on the 0.9 m Na₂CO₃ solutions were conducted at 0.2 GPa, 823 K and 11 GPa, 1000 K. Two xc functionals were compared: PBE and PBE0.

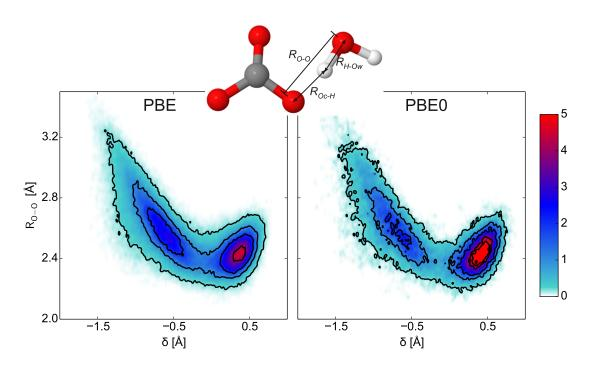


Figure 4: Probability distributions of positions of protons hopping between CO_3^{2-} and H_2O in the Na₂CO₃ solution at 11 GPa and 1000 K. The unit is Å⁻². The reaction coordinate R_{O-O} is the distance between the two neighboring oxygen atoms, O_c and O_w , in carbonate ions and water molecules respectively, and δ is the proton displacement $R_{Oc-H} - R_{H-Ow}$. Two xc functionals were compared: PBE and PBE0.